VARIFORC processing examples

Rectangular hysteresis

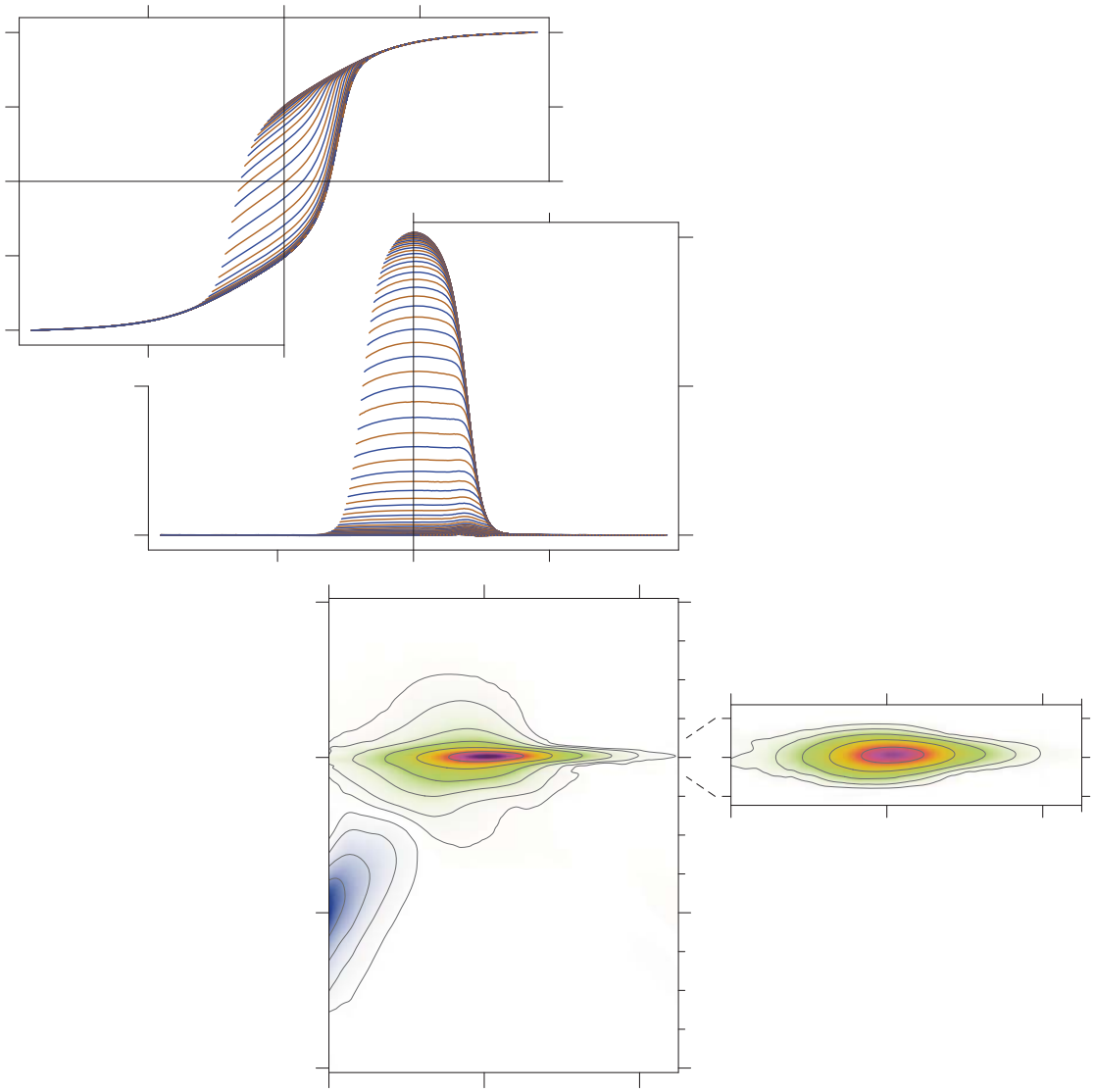

About this example

The measured material consists of dried cells of the magnetotactic bacterium MV-1. FORC measurements were kindly provided by H. Wang and are reported in *Wang et al.* [2013]. MV-1 produces a single chain of ~10 prismatic magnetite crystals (magnetosomes), ~35×53 nm in size on average, with the long crystal axis parallel to the chain axis [*Sparks et al.*, 1990]. Each chain is magnetically equivalent to one elongated single-domain particle [*Dunin-Borkowski et al.*, 2001; *Egli et al.*, 2010] with tightly constrained magnetic anisotropy arising from precise biological control on size, shape and distance between crystals. Magnetosome chains are separated from each other by the much larger cell volume, so that magnetostatic interactions between chains are largely avoided.

Because of strict control over domain state, magnetic anisotropy, and distance between chains, the dried MV-1 culture behaves as an ideal assemblage of identical, uniaxial single-domain particles, whose magnetic properties are described by *Stoner and Wohlfarth* [1948] and *Newell* [2005]. The corresponding hysteresis loop is characterized by steep branches, and this property is reflected by FORC measurements being highly sensitive to applied fields in proximity of the positive and negative coercive field. This sensitivity poses specific FORC processing problems, which require a limitation of the smoothing factor over regions where first derivatives of the measured curves are maximal.

FORC measurements

- Measuring instrument: PMC MicroMag 2900 AGM.
- Specimen preparation: Unknown.
- FORC measurement protocol:

```
Hc1 = 0      , Hc2 = 0.12 T
Hb1 = -0.12 T, Hb2 = +0.06 T
Hsat = 1.0 T
Averaging time       = 0.2 s
Pause at calibration = 1.0 s
Pause at reversals   = 1.0 s
Pause at saturation  = 1.0 s
Smoothing = 5 (adds a 5-point margin to the measured range)
```

- Derived measurement parameters:

```
Number of curves: 513
Calibration measurements at 0.187 T
Mean size of field steps = 0.60 mT (maximum resolution of the FORC diagram)
```

- **Notes on measurements.** None.

About VARIFORC processing options used in this example

VARIFORC modules are controlled by processing options stored in so-called parameter files. Parameter files used to process FORC data related to this example can be find in the folder containing this document. These are:

1. Import and correct FORC measurements (`ImportFORC` module):

- `MV1_VARIFORC_ImportFORC_parameters.txt`: without first-point correction.
- `MV1-fpc_VARIFORC_ImportFORC_parameters.txt`: with first-point correction.

2. Calculate the FORC diagram (`CalculateFORC` module):

- `MV1-SF3_VARIFORC_CalculateFORC_parameters.txt`: conventional processing with constant smoothing factor (SF = 3). For demonstration purposes only.
- `MV1-vari_VARIFORC_CalculateFORC_parameters.txt`: variable smoothing with smoothing factor limitation along the central ridge. For demonstration purposes only.
- `MV1-opt_VARIFORC_CalculateFORC_parameters.txt`: variable smoothing with smoothing factor limitation along the central ridge and along diagonals with maximum first-derivative amplitudes.

3. Isolate the central ridge (`IsolateCR` module):

- `MV1-auto_VARIFORC_IsolateCR_parameters.txt`: central ridge isolation with automatic options.
- `MV1-manual_VARIFORC_IsolateCR_parameters.txt`: central ridge isolation with manually optimized parameters.

FORC measurements

High-resolution measurements have been imported and corrected with **ImportFORC** (see parameter file `MV1_VARIFORC_ImportFORC_parameters.txt`). In many cases, the first measurement of each curve lies above the trend set by the other points (see VARIFORC example on first-point correction). This effect is barely visible in this example (Plates 1a,b), so that a correction of first-point measurements with VARIFORC is not necessary. Indeed, a first-point correction (see parameter file `MV1-fpc_VARIFORC_ImportFORC_parameters.txt`) does not produce noticeable effects (Plates 1c,d). This example confirms that the first-point correction procedure used by VARIFORC does not introduce, by itself, any artifacts.

The hysteresis loop formed by the envelope of the measured curves bears the typical signature of randomly oriented uniaxial single-domain particles [*Stoner and Wohlfarth*, 1948]. The steep flanks of the two loop branches indicate that particles have nearly identical magnetic anisotropies associated which a narrow coercivity distribution. In general, the area enclosed by a rectangular hysteresis loop is difficult to cover with FORC measurements, since curves tend to accumulate in proximity of the upper and lower hysteresis branches. Therefore, very small field steps are needed for adequate coverage of the whole hysteresis loop.

The envelope of measurement curves from which the lower hysteresis branch has been subtracted (Plates 1b,d) coincides with the even component of the hysteresis loop, i.e. the difference between upper and lower branches [*Fabian and Dobeneck*, 1997]. Individual curves starting at negative reversal fields ($H_r < 0$) run relatively flat until they reach the right end of the envelope, where $H = -H_r$ and the curve slope changes sharply. This typical signature of non-interacting single-domain particles generate FORC diagrams containing a so-called central ridge [*Egli et al.*, 2010].

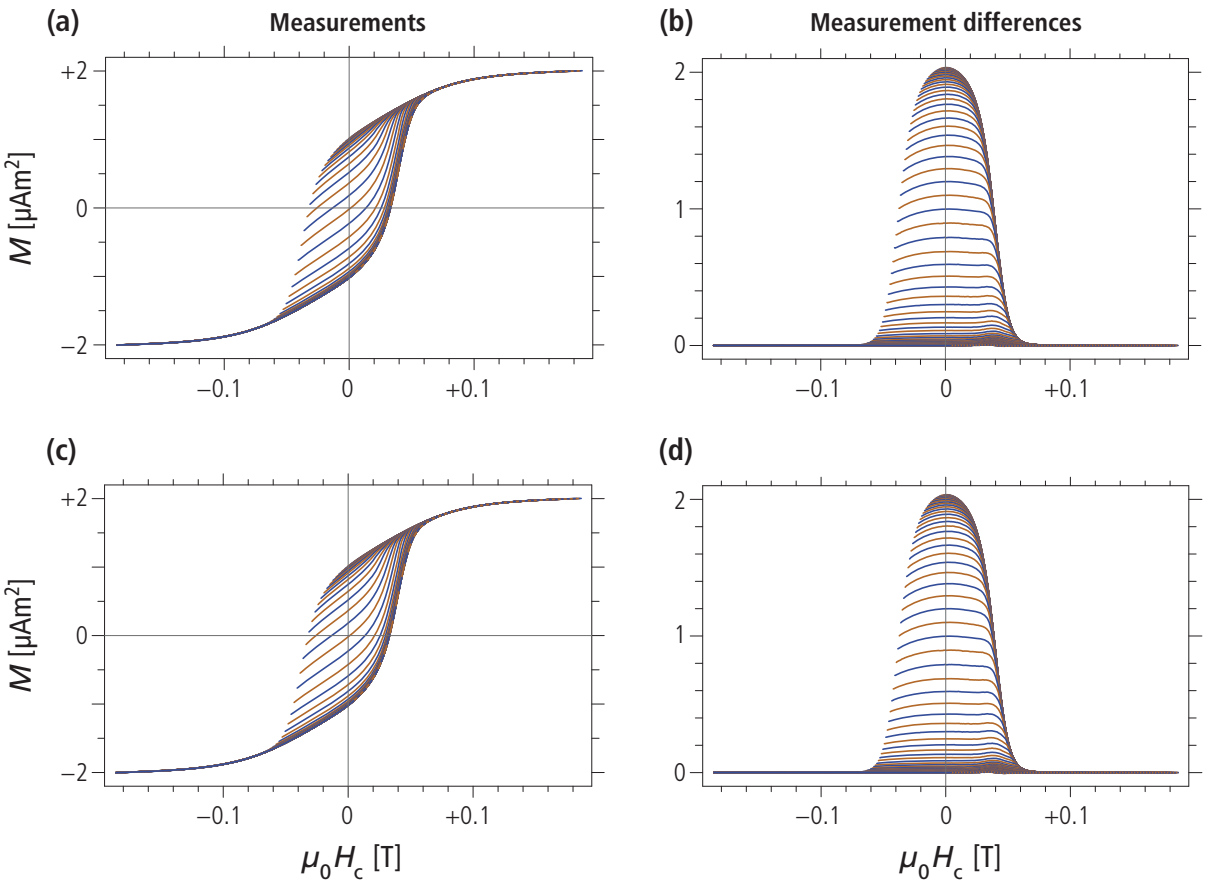

Plate 1. FORC measurements. (a-b) Drift- and outlier-corrected measurements. **(c-d)** Same as (a-b) with first-point correction. Plots were generated by **`ImportFORC`** with minor editing. Left plots show the measured curves, (every 4th curve for clarity, see `INPUT 14` of the parameter file). Right plots show the same measurements after subtraction of the lower hysteresis branch reconstructed from the FORC measurements (see `INPUT 21` of the parameter file). Every 2rd curve is shown for clarity. Notice that only ~30 out of a total of 513 measured curves are visually distinguishable from the two branches of the hysteresis loop.

Hysteresis properties of this sample ($M_{rs}/M_s = 0.495$ and $H_{cr}/H_c = 1.19$) match almost perfectly those of randomly oriented, single-domain particles with uniaxial anisotropy (Plate 2). Similar results are systematically obtained with intact magnetotactic bacteria cultures (green dots), and represent one end-member for the hysteresis properties of magnetofossil-bearing sediments.

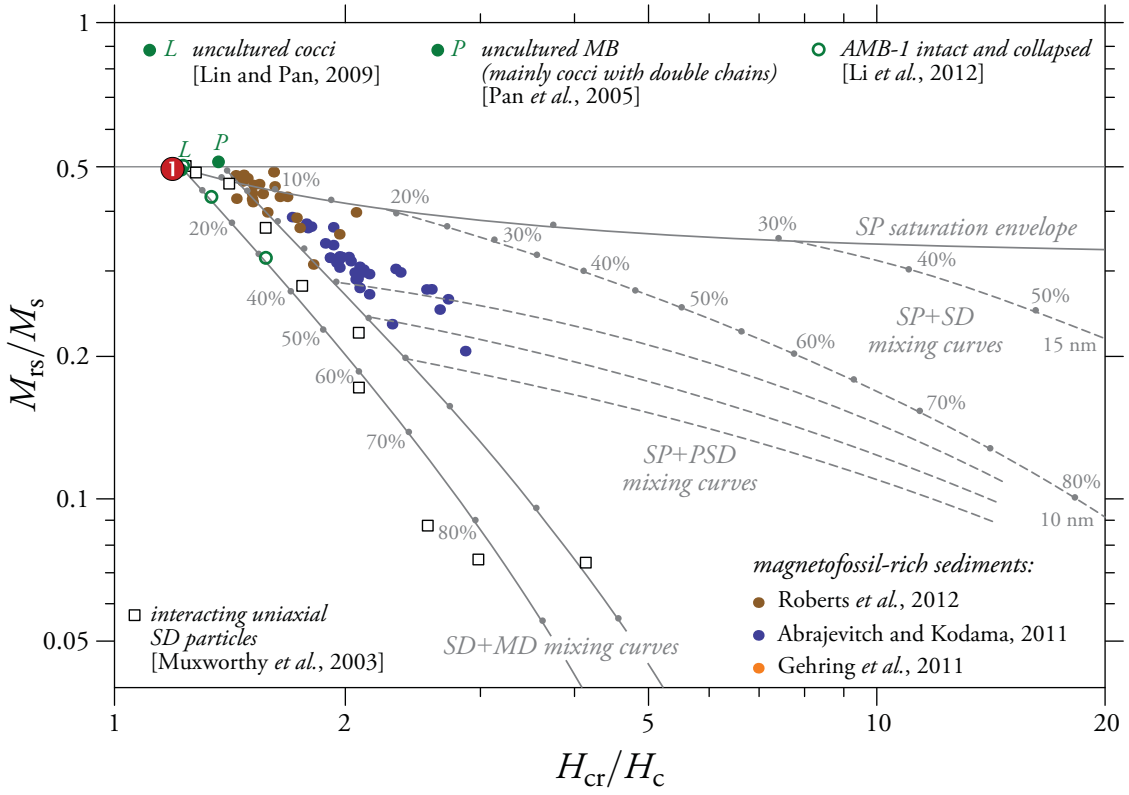

Plate 2. Hysteresis parameters in the Day diagram. Day diagram after *Dunlop* [2002] showing the hysteresis properties of the MV-1 culture (❶).

Optimized FORC diagram calculation

This example shows how to process FORC data of samples with a rectangular hysteresis loop without introducing oversmoothing artifacts, while still providing excellent results in terms of measurement noise suppression. As seen in previous section, rectangular hysteresis loops are characterized by very steep branches near the positive and negative coercive fields ($\pm H_{coerc}$). Consequently, first derivatives with respect to the field at which each curve begins ($\partial M/\partial H_r$) and the applied field during measurements ($\partial M/\partial H$) become very large in proximity of $H_r = -H_{coerc}$ and of $H = +H_{coerc}$, respectively. Here, high resolution – and therefore a small smoothing factor – is needed to fit rapid magnetization changes without introducing polynomial regression artifacts. VARIFORC can automatically handle the required smoothing factor limitations around $\pm H_{coerc}$ in order to avoid processing artifacts, as shown in the following.

Plate 3a,b shows the result of conventional FORC processing with a constant smoothing factor SF = 3 (see the parameter file `MV1-SF3_VARIFORC_ImportFORC_parameters.txt`). Measurement noise is evident in this FORC diagram, especially on lower contours. Attempts to reduce the noise level by increasing the smoothing factor, for instance using the typical smoothing parameters applicable to magnetofossil-bearing sediments (see the parameter file `MV1-vari_VARIFORC_ImportFORC_parameters.txt`), introduce evident processing artifacts along the diagonals defined by $H_r = -H_{coerc}$ and $H = +H_{coerc}$ (Plate 3c,d). These artifacts originate from excessive smoothing over portions of the measured curves with maximum first derivative amplitudes.

Smoothing artifacts will appear with any type of sample if the smoothing factor is increased beyond a certain limit, which depends on hysteresis properties. Samples with rectangular hysteresis loops are particularly susceptible to this problem. In such cases, VARIFORC can limit the smoothing factor along diagonals of the FORC space with maximum $\partial M/\partial H_r$ and $\partial M/\partial H$ amplitudes (see `INPUT 14` in the parameter file `MV1-opt_VARIFORC_ImportFORC_parameters.txt`). The task is fully automatized, so that the user is only required to enter the maximum smoothing factor allowed over critical regions (manual control is also possible, see Chapter 4 of the VARIFORC user manual). When this option is used, the size of rectangular regions chosen for local polynomial regression is limited around suitably chosen diagonals (Plate 3e), so that the resulting FORC diagram is free from smoothing artifacts while still providing a high degree of measurement noise suppression (Plate 3f). Notice that the smallest contour level in Plate 3f is <0.5% of the central peak amplitude and still significant, while amplitudes <5% are not significant in the FORC diagram obtained with conventional processing (Plate 3a).

Key for the correct application of the advanced smoothing options provided by VARIFORC is the correct identification of smoothing artifacts, as explained in the next section. The appearance of smoothing artifacts – sometimes even with conventional processing – depends strongly on the material being analyzed. Samples whose magnetization is very sensitive to small field changes are particularly prone to oversmoothing problems, which, however, can be solved with the smoothing factor limitation options of **`CalculateFORC`** (see Chapter 4 of the VARIFORC user manual).

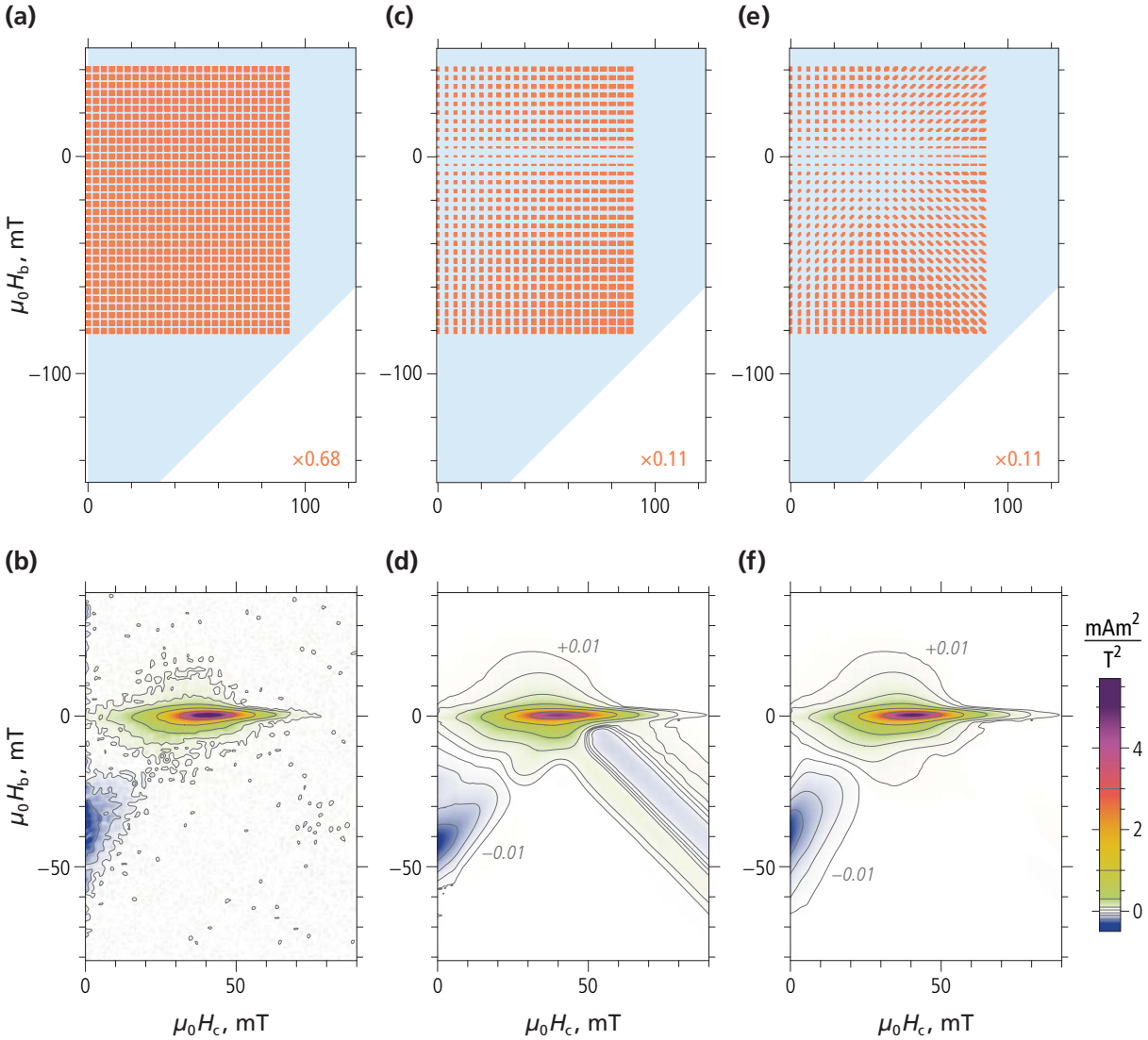

Plate 3. Smoothing parameter optimization in case of rectangular hysteresis. The top graphics row shows rectangular selections (orange, not to scale) of measurement points (shaded blue area) used for polynomial regression. The size of these rectangular selection is controlled by a horizontal (s_c) and a vertical (s_b) smoothing factor, with additional diagonal limits applied by some options. This is a standard representation of regression rectangles, as shown by **`CalculateFORC`**. The bottom graphics row shows the resulting FORC diagrams (contour lines have been added with **`PlotFORC`**). The same color scale has been used for all diagrams. **(a,b)** Conventional FORC processing with a constant smoothing factor SF = 3 (parameter file: `MV1-SF3_VARIFORC_ImportFORC_parameters.txt`). **(c,d)** FORC processing based on variable smoothing options commonly used to process magnetofossil-bearing sediments (`MV1_vari_VARIFORC_ImportFORC_parameters.txt`). The size of regression rectangles increases proportionally to the distance from the FORC diagram axes, starting from $s_c = 9$ at $H_c = 0$ and $s_b = 9$ at $H_b = 0$. An extra limit of $s_b = 3$ is applied along $H_b = 0$ for a better resolution of the central ridge. Notice the smoothing artifacts along diagonals departing from the central maximum over the lower quadrant of the FORC diagram. **(e,f)** Same as (c,d), after limiting the size of regression rectangles over diagonals where smoothing artifacts appeared in (d). The diagonal smoothing factor limit was set to SF = 9 (`MV1_opt_VARIFORC_ImportFORC_parameters.txt`). Smoothing factor artifacts are completely absent in this case.

Recognizing processing artifacts

Unfortunately, a universal method for maximizing measurement noise suppression while keeping the necessary resolution and avoiding FORC processing artifacts does not exist. The FORC processing examples discussed in the last section shows the importance of artifact identification. For this purpose, plots of the standard error associated with the FORC diagram are provided as part of the standard `CalculateFORC` output (see Chapter 4 of the VARIFORC user manual). These error plots are shown in Plate 4 for the same FORC diagrams discussed in the last section. The standard error is estimated from the misfit of polynomial regression, which arises from measurement errors, as well as oversmoothing, i.e. the incapability of a second-order polynomial to reproduce parts of the measurement curves over intervals set by the chosen smoothing options [*Heslop and Roberts*, 2012].

Measurement errors are characterized by a relatively constant background with a diagonal texture reflecting the orientation of the measurement point grid (❶ in Plate 4b). In some cases, the amplitude of measurement errors increases towards large values of H_c, due to electromagnet noise being recorded by the measurement system. Larger measurement errors might occur at the edges of the measurement range, especially along $H_c = 0$ (❷ in Plate 4b), where the sudden change of the field sweep rate might produce anomalous measurements (see VARIFORC example on first-point correction). Diagonal stripes with elevated measurement errors (❸ in Plate 4b) occur along the traces of individual curves affected by some transient instabilities. Overall, measurement noise is characterized by patterns that are unrelated to the FORC diagram, or any property of the sample being measured.

FORC processing artifacts, on the other hand, occur at places where local polynomial regression cannot fit the measured curves adequately, as for instance along the central ridge (❹ in Plate 4b), where the slope of measured curves changes abruptly. Processing artifacts are sometimes related to features of the measured curves that are not visible in the FORC diagram, such as first-derivative maxima along diagonals corresponding to $H_r = -H_{coerc}$ and $H = +H_{coerc}$ (❺ in Plate 4b). In general, suspect FORC diagram features (e.g. ❺ in Plate 4c) matching elevated standard errors should be considered as processing artifacts to be removed with proper smoothing factor limitations, and, if necessary, by increasing the measurement resolution.

The acceptance limit for regression errors depends on corresponding amplitudes in the FORC diagram. For example, the maximum error (❹) over the central ridge in Plate 4d is ~10 times larger than the error (❺) associated with first derivative maxima, yet only the latter error source produces unacceptable FORC diagram artifacts (Plate 4c). This is because errors marked with ❺ overlap with small intrinsic FORC amplitudes, while errors marked with ❹ are still ~25 times smaller than the central ridge amplitude.

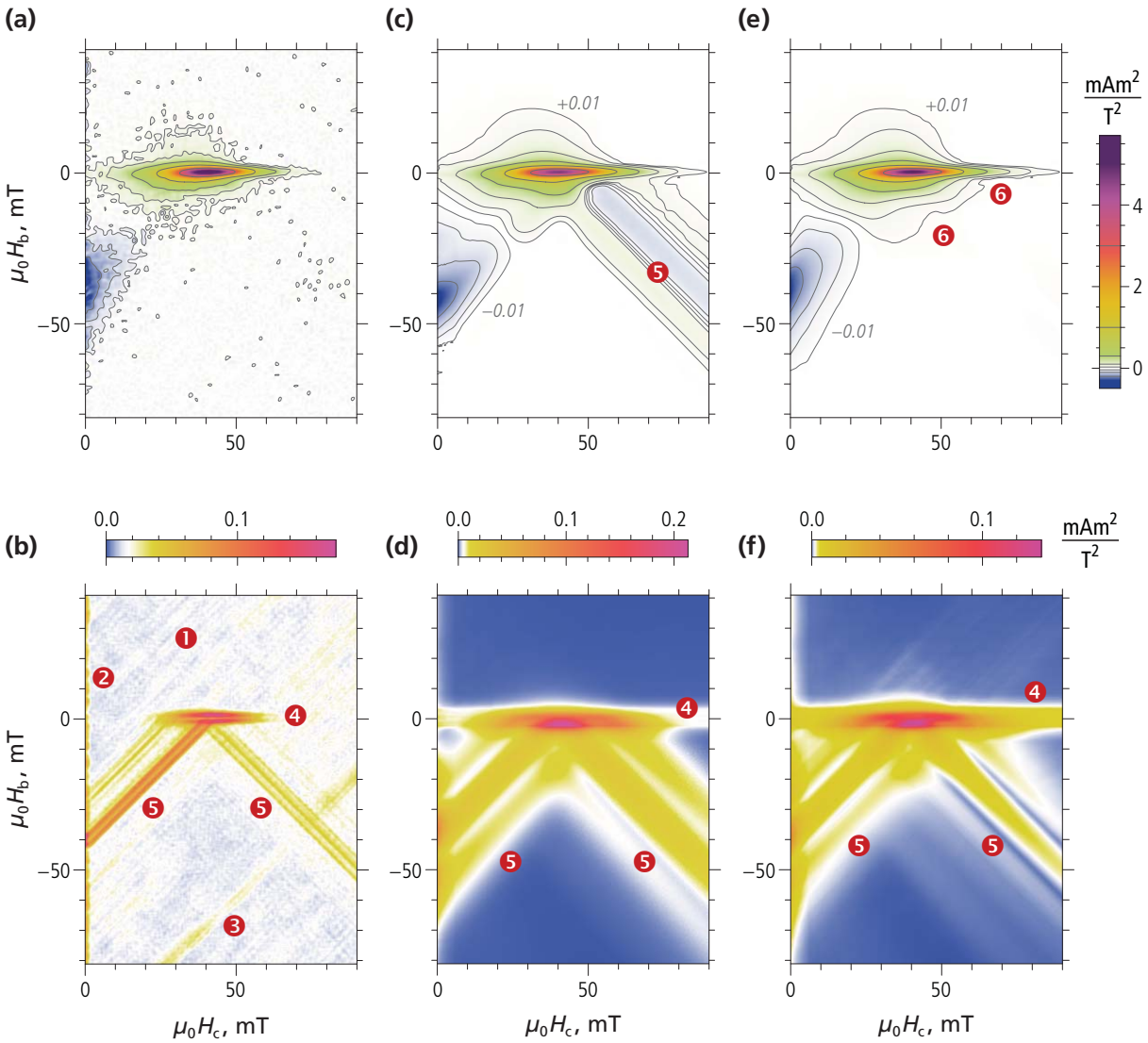

Plate 4. Measurement noise and processing artifacts in FORC diagrams. FORC diagrams (first row) and corresponding standard error estimates after *Heslop and Roberts* [2012], as generated by **`CalculateFORC`** (second row). Same processing parameters have been used as in Plate 3. The color scale of error plots is chosen so, that white corresponds to the mean standard error. Accordingly, blue and yellow-red regions are characterized by error levels that are below and above the average, respectively. Following error patterns are highlighted: ❶ normal measurement noise level, ❷ enhanced measurement errors along $H_c = 0$, ❸ enhanced measurement errors along the trace of unstable curves, ❹ enhanced error due to polynomial misfits under the central ridge, ❺ enhanced error due to polynomial misfits under first-derivative maxima. **(a,b)** Measurement noise (❶) is directly visible in the FORC diagram due to undersmoothing. **(c,d)** Measurement noise is adequately suppressed, but oversmoothing artifacts (❺) appear in the FORC diagram. **(e,f)** Processing artifacts marked with ❺ have been reduced by limiting the smoothing factor along diagonals corresponding to $H_r = -H_{coerc}$ and $H = +H_{coerc}$. The maximum amplitude of the standard error associated with these artifacts corresponds to the smallest contour level in the FORC diagram, i.e. ~0.01 mAm^2/T^2. The two indentations of the corresponding contour line (❻) are produced by residual processing artifacts. All the other contours, are free of measurement noise and oversmoothing artifacts, providing an exact representation of the FORC function.

Complete VARIFORC analysis

A summary of FORC properties typical for intact magnetotactic bacteria is shown in plate Plate 5. The central ridge is the dominant feature of the FORC diagram (Plate 5a), as expected for this kind of samples. The isolated ridge (Plate 5c) shows some broadening due to residual magnetostatic interactions which is not seen in magnetofossil-rich sediments (see corresponding VARIFORC example). This means that fossil magnetosome chains are better dispersed inside the sediment matrix than in this example, where the minimum separation between chains corresponds to the size of dried cells.

FORC contributions remaining after central ridge removal (Plate 5b), contain the typical signature of reversible magnetic moment rotation in uniaxial single domain particles, in form of a pair of negative and positive regions over the lower quadrant, which are (nearly) symmetric about the $H_b = -H_c$ diagonal [*Newell*, 2005; *Egli et al.*, 2010]. On the other hand, positive FORC contributions over the upper quadrant are incompatible with non-interacting single-domain particles and are probably produced by a small fraction of collapsed chains. A similar signature is also seen in magnetofossil-rich sediments, even after removing non-single-domain contributions by selective chemical dissolution (see corresponding VARIFORC example).

Coercivity distributions derived from FORC measurements and from the central ridge (Plate 5d) are unusually narrow, reflecting the strong biological control over properties of magnetosome chains that control coercivity, such as magnetosome elongation, separation between consecutive magnetosomes, and chain length. The coercivity distribution f_{ir} corresponding to irreversible processes along the lower branch of the hysteresis loop is strictly positive (i.e., $f_{ir} = 0$ for negative arguments), as expected from non-interacting single-domain particles. This condition is not met by magnetofossils, due to broader coercivity distributions and, possibly, to a higher degree of chain collapse.

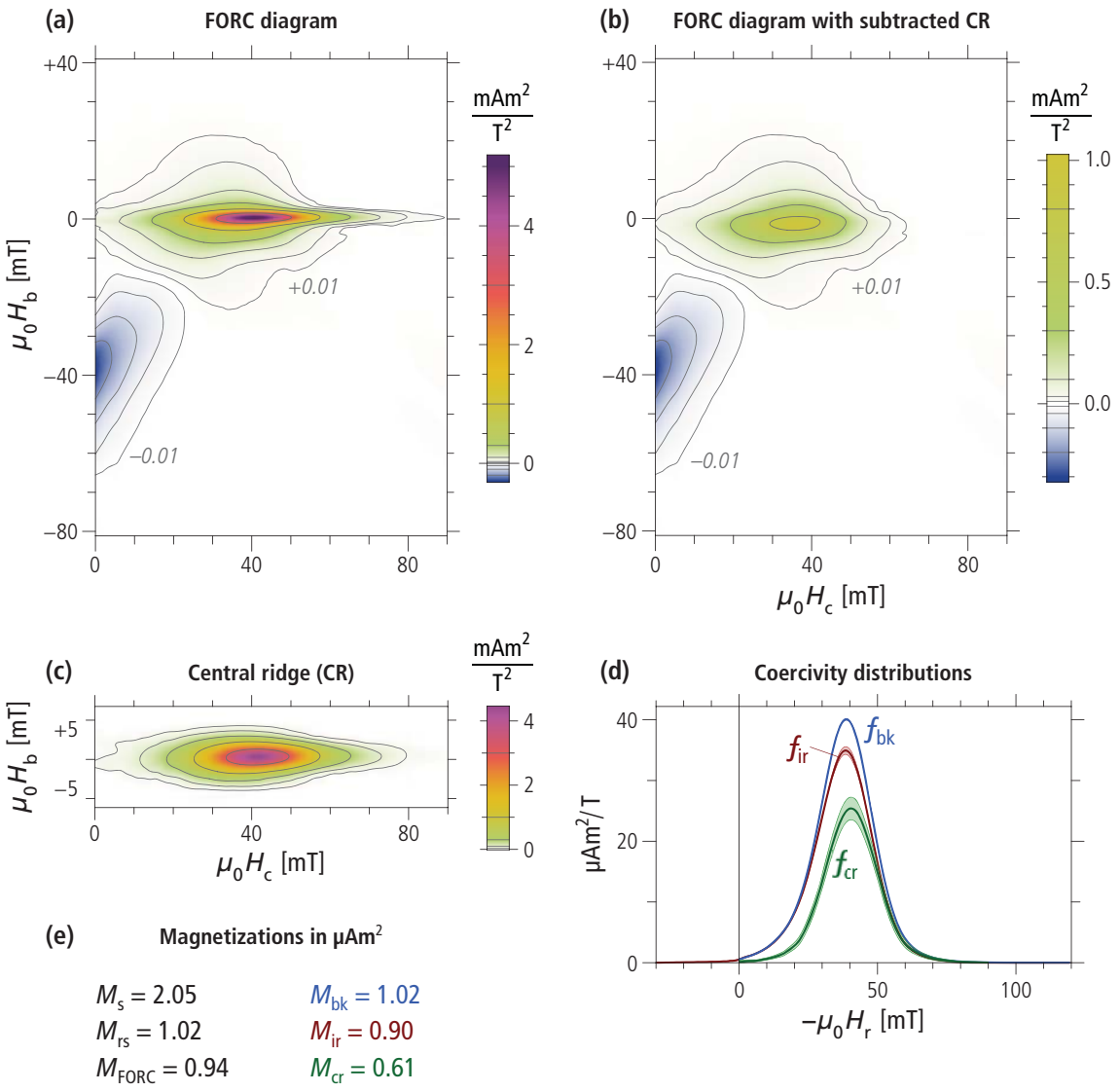

Plate 7. Complete VARIFORC analysis of MV-1 magnetosome chains. (a) FORC diagram obtained with **`CalculateFORC`** (contour lines have been added with **`PlotFORC`**). Notice that the smallest contour level corresponds to 0.5% of the maximum FORC amplitude and is still fully significant. **(b)** FORC diagram remaining after subtraction of the central ridge with **`IsolateCR`**. The isolated central ridge is shown in **(c)** with a 2× vertical exaggeration, which highlights a small upward shift of the whole ridge, as well as some broadening due to residual magnetostatic interactions between chains. All FORC diagrams share the same color scale. **(d)** Three types of coercivity distribution derived from FORC measurements, with shaded bands around each curve representing 2σ confidence levels. The first two distributions, f_{bk} and f_{ir}, originate from FORC measurements in $H = 0$ and from the irreversible component of the lower branch of the hysteresis loop, respectively. They are generated by **`CalculateFORC`** as part of the standard output. The third distribution, f_{cr}, is associated with the central ridge and is generated by **`IsolateCR`**. All three distributions are plotted by **`IsolateCR`** as seen in this example. f_{ir} is the only distribution that exists for positive and negative fields, like the hysteresis loop from which it is derived. Negative arguments of f_{ir} originate from irreversible magnetization processes that occur without reversing the field direction. Only non-interacting, uniaxial single-domain particles produce a strictly positive f_{ir}. **(e)** Total magnetizations derived from FORC measurements (M_s and M_{rs}), integration of the FORC diagram (M_{FORC}), and integration of the coercivity distributions shown in (d) (M_{bk}, M_{ir}, and M_{cr}).

Literature

Abrajevitch, A., K. Kodama (2011). Diagenetic sensitivity of paleoenvironmental proxies: A rock magnetic study of Australian continental margin sediments, *Geochemistry, Geophysics, Geosystems 12*, Q05Z24, doi:101029/2010GC003481.

Dunin-Borkowski, R.E., M.R. McCartney, M. Pósfai, R.B. Frankel, D.A. Bazylinski, and P.R. Buseck (2001). Off-axis electron holography of magnetite bacteria: magnetic microstructure of strains MV-1 and MS-1, *European Journal of Mineralogy 13*, 671-684.

Dunlop, D.J. (2002). Theory and application of the Day plot (M_{rs}/M_s versus H_{cr}/H_c) 2. Application to data for rocks, sediments, and soils, *Journal of Geophysical Research 107*, 2057, doi:10.1029/2001JB000487.

Egli, R., A.P. Chen, M. Winklhofer, K.P. Kodama, C.S. Horng (2010). Detection of noninteractinig single domain particles using first-order reversal curve diagrams, *Geochemistry, Geophysics, Geosystems 11*, Q01Z11, doi:101029/2009GC002916.

Fabian, K., T. von Dobeneck (1997). Isothermal magnetization of samples with stable Preisach function: A survey of hysteresis, remanence, and rock magnetic parameters, *Journal of Geophysical Research 102*, 17659-17677.

Gehring, A.U., J. Kind, M. Charilaou, I. García-Rubio (2011). The detection of magnetotactic bacteria and magnetofossils by means of magnetic anisotropy, *Earth and Planetary Science Letters 309*, 113-117.

Heslop, D., and A.P. Roberts (2012). Estimation of significance levels and confidence intervals for first-order reversal curve distributions, *Geochemistry, Geophysics, Geosystems 13*, Q12Z40, doi:101029/2012GC 004115.

Li, J., W. Wu, Q. Liu, and Y. Pan (2012). Magnetic anisotropy, magnetostatic interactions, and identification of magnetofossils, *Geochemistry, Geophysics, Geosystems 13*, Q10Z51, doi:101029/2012GC004384.

Lin, W., Y. Pan (2009). Uncultivated magnetotactic cocci from Yuandadu Park in Beijing, China, *Applied and Environmental Microbiology 75*, 4046-4052.

Muxworthy, A., W. Williams, D. Virdee (2003). Effect of magnetostatic interactions on the hysteresis parameters of single-domain and pseudo-single-domain grains, *Journal of Geophysical Research 108*, doi:10.1029 /2003JB002588.

Newell, A.J. (2005). A high-precision model of first-order reversal curve (FORC) functions for single-domain ferromagnets with uniaxial anisotropy, *Geochemistry, Geophysics, Geosystems 6*, Q05010, doi:101029/ 2004GC000877.

Pan, Y., N. Petersen, M. Winklhofer, A.F. Davila, Q. Liu, T. Frederichs, M. Hanzlik, R. Zhu (2005). Rock magnetic properties of uncultured magnetotactic bacteria, *Earth and Planetary Sciences 237*, 311-325.

Roberts, A.P., L. Chang, D. Heslop, F. Florindo, J.C. Larrasoaña (2012). Searching for single domain magnetite in the "pseudo-single-domain" sedimentary haystack: Implications of biogenic magnetite preservation for sediment magnetism and relative paleointensity determination, *Journal of Geophysical Research 117*, B08104, doi:10.1029/2012JB009412.

Sparks, N.H.C., S. Mann, D.A. Bazylinski, D.R. Lovley, H.W. Jannasch, R.B. Frankel (1990). Structure and morphology of magnetite anaerobically-produced by a marine magnetotactic bacterium and a dissimilatory iron-reducing bacterium, *Earth and Planetary Science Letters 98*, 14-22.

Stoner, E.C., and E.P. Wohlfarth (1948). A mechanism of magnetic hysteresis in heterogeneous alloys, *Philosophical Transactions of the Royal Society of London, A240*, 599-642.

Wang, H., D.V. Kent, M.J. Jackson (2013). Evidence for abundant isolated magnetic nanoparticles at the Paleocene-Eocene boundary, *Proceedings of the National Academy of Sciences of the United States 110*, 425-430, doi:10.1073/pnas.1205308110.